

Marine-Atmospheric Boundary Layer Characteristics over the South China Sea During the Passage of Strong Typhoon Hagupit

CHENG Xueling¹ (程雪玲), WU Lin¹ (吴琳), SONG Lili² (宋丽莉), WANG Binglan² (王丙兰),
and ZENG Qingcun^{3*} (曾庆存)

¹ State Key Laboratory of Atmospheric Boundary Layer Physics and Atmospheric Chemistry, Institute of Atmospheric Physics, Chinese Academy of Sciences, Beijing 100029

² Public Weather Service Center, China Meteorological Administration, Beijing 100081

³ Institute of Atmospheric Physics, Chinese Academy of Sciences, Beijing 100029

(Received December 10, 2013; in final form January 8, 2014)

ABSTRACT

The structures and characteristics of the marine-atmospheric boundary layer over the South China Sea during the passage of strong Typhoon Hagupit are analyzed in detail in this paper. The typhoon was generated in the western Pacific Ocean, and it passed across the South China Sea, finally landfalling in the west of Guangdong Province. The shortest distance between the typhoon center and the observation station on Zhizi Island (10 m in height) is 8.5 km. The observation data capture the whole of processes that occurred in the regions of the typhoon eye, two squall regions of the eye wall, and weak wind regions, before and after the typhoon's passage. The results show that: (a) during the strong wind (average velocity $\bar{u} \geq 10 \text{ m s}^{-1}$) period, in the atmospheric boundary layer below 110 m, \bar{u} is almost independent of height, and vertical velocity \bar{w} is greater than 0, increasing with \bar{u} and reaching 2–4 m s^{-1} in the squall regions; (b) the turbulent fluctuations (frequency $> 1/60 \text{ Hz}$) and gusty disturbances (frequency between 1/600 and 1/60 Hz) are both strong and anisotropic, but the anisotropy of the turbulent fluctuations is less strong; (c) \bar{u} can be used as the basic parameter to parameterize all the characteristics of fluctuations; and (d) the vertical flux of horizontal momentum contributed by the average flow ($\bar{u} \cdot \bar{w}$) is one order of magnitude larger than those contributed by fluctuation fluxes ($\overline{u'w'}$ and $\overline{v'w'}$), implying that strong wind may have seriously disturbed the sea surface through drag force and downward transport of eddy momentum and generated large breaking waves, leading to formation of a strongly coupled marine-atmospheric boundary layer. This results in $\bar{w} > 0$ in the atmosphere, and some portion of the momentum in the sea may be fed back again to the atmosphere due to $\bar{u} \cdot \bar{w} > 0$.

Key words: Typhoon Hagupit, marine-atmospheric boundary layer, turbulent fluctuation, gusty disturbance, air-sea interaction, South China Sea

Citation: Cheng Xueling, Wu Lin, Song Lili, et al., 2014: Marine-atmospheric boundary layer characteristics over the South China Sea during the passage of strong Typhoon Hagupit. *J. Meteor. Res.*, **28**(3), 420–429, doi: 10.1007/s13351-014-3279-0.

1. Introduction

Oceans occupy two-thirds of the world's surface, and the influence of air-sea interaction on weather process and climate change is much more significant than that of land-atmosphere interaction (Ola et al., 2005). The disastrous weather and climate phenomena in marine areas are more severe than those in land areas.

However, due to the limitation of observational conditions, it is difficult to make measurements of the marine-atmospheric boundary layer. Thus, to date, observations and studies of the marine-atmospheric boundary layer remain inadequate, especially for situations involving strong winds. Most existing work concerning the marine-atmospheric boundary layer has involved applying the results obtained in laboratory-

Supported by the National Natural Science Foundation of China (40830103 and 91215302), National (Key) Basic Research and Development (973) Program of China (2010CB951804), China Meteorological Administration Special Public Welfare Research Fund (GYHY201306057), and Strategy Guide for the Specific Task of the Chinese Academy of Sciences (XDA10010403).

*Corresponding author: zqc@mail.iap.ac.cn.

©The Chinese Meteorological Society and Springer-Verlag Berlin Heidelberg 2014

based fluid dynamics experiments and atmospheric boundary layer station observations. The laws governing the characteristics of the marine-atmospheric boundary layer under windy conditions have not yet been clearly revealed. Actually, strong wind occurs much more frequently above the oceanic surface than above the land surface. Driven by the strong wind, the oceanic surface current and breaking waves together with the atmospheric motion form a coupled marine-atmospheric boundary layer, constituting a complicated air-sea system.

In the past two decades, due to increased interest in tropical storms, hurricanes, and their formation and evolution, as well as the significant impact of strong winds on marine engineering and operation, atmospheric and oceanographic scientists, along with structural engineers, have made some important observations and analyses of strong marine winds, especially those associated with hurricanes and typhoons. Although such observations have largely been made on a case-by-case basis, they are still extremely valuable. Observations of this kind are mostly performed by dropsonde, aircraft, Doppler radar, and so on (e.g., Franklin et al., 2002; Powell et al., 2003; Schroeder and Douglas, 2003; Knupp et al., 2005; Abernethy et al., 2006; French et al., 2007; Kudryavtsev and Makin, 2007; Sanford et al., 2007; Zhang et al., 2008; Zedler et al., 2009). Some valuable directly observed data have also been obtained during typhoon landfalls and when tropical cyclones passing over islands or marine observational platforms (Sparks, 2001; Xu and Zhan, 2001; Song et al., 2005, 2010; Harper, 2008; Cao et al., 2009; Li et al., 2010; Chen et al., 2011; Liu et al., 2011; Peng et al., 2012; Xiao et al., 2012). In particular, the works of Song et al. (2005, 2010) were based on strong typhoons such as Damrey, Nuri, Chunchi, Prapiroon, Hagupit, and so on. They focused on studying the engineering problems faced by structures such as buildings, bridges, and wind power installations.

Using the data of Song et al. (2005, 2010), in this paper we focus on the marine-atmospheric boundary layer characteristics, such as those concerning turbulence and wind gusts, and their parameterization. We will employ our own specially developed method,

which has already been successfully applied to the previous studies of the boundary layer during strong winds related to sand storms and cold surges (Zeng, 2006; Cheng et al., 2007; Zeng et al., 2010; Cheng et al., 2011, 2012a, b). We divide the fluctuations (or turbulences) into two parts, one being high-frequency turbulent fluctuation (frequency higher than 1/60 Hz), and the other being gusty wind disturbance (frequency between 1/600 and 1/60 Hz). The two parts have different structures and play different roles, such as in the transport of heavy aerosol particles (Zeng, 2006; Zeng et al., 2010; Cheng et al., 2012b). Meanwhile, by comparing with strong cold-surge cases (Cheng et al., 2014), we show that there are many common features in the marine-atmospheric boundary layer under strong winds.

2. Data and instruments

In China, there are many marine meteorological observational stations in the coastal areas of Guangdong Province and over the islands of the South China Sea. Certain stations play host to periods of denser and one-off observational campaigns during the typhoon season to monitor the landfalling of particular typhoons of interest. The station on Zhizi Island is one such station. The data used in this study were mainly obtained from Zhizi (additional data from some other coastal meteorological stations were also used). For a detailed description of this station and its instruments, readers can refer to Liu et al. (2011) and Xiao et al. (2012). However, for convenience, a brief overview is provided as follows.

Zhizi Island is located off the coast of Bohe, Maoming City. The shortest offshore distance is 4.6 km, and the exposed part of the island is about 90 m long and 40 m wide (Fig. 1). The observation tower on Zhizi is 100 m high at 21°27'23"N, 111°22'28"E, and the base altitude is 10 m above sea level. The surrounding water depth is 6–10 m. There are 6 sets of cup anemometers (NRG-Symphonie type) installed at heights of 10, 20, 40, 60, 80, and 100 m on the tower, and 3 sets of wind direction observation instruments at heights of 10, 60, and 100 m. In the typhoon season



Fig. 1. Location of Zhizi Island and trajectory of Typhoon Hagupit (after Liu et al., 2011).

from August 2008 to August 2010, there was also one ultrasonic anemometer at 60-m height (Gill-Windmaster Pro.; sampling frequency 10 Hz).

3. Typhoon Hagupit and its structure and development

Typhoon Hagupit formed on 19 September 2008 in the western Pacific Ocean near the Philippines. It moved westward and strengthened into a strong typhoon, and landed at 0645 BT 24 September near Chen Village, Bohe, Maoming City, Guangdong Province (Liu et al., 2011; Xiao et al., 2012). The trajectory of Hagupit is shown in Fig. 1. The shortest distance between the typhoon center and Zhizi station is 8.5 km. During the typhoon's landing, the 10-min averaged wind speed reached force 15 (48.5 m s^{-1}) at Bohe meteorological station near Zhizi, and the 3-s instant maximum gust reached 63.9 m s^{-1} , as observed at 60-m level of the Zhizi tower. The lowest surface

pressure was 956 hPa, which lasted for 8 min (Song et al., 2010; Liu et al., 2011; Xiao et al., 2012).

There have been many detailed analyses of the 10-min averaged velocity characteristics and turbulent statistics of Hagupit (Song et al., 2010; Liu et al., 2011; Xiao et al., 2012), but the goals of these studies were to examine the typhoon's effects on engineering structures. Based on these works, we reanalyzed the original data with added quality control tests. The 10-min averaged wind velocities (\bar{u} , \bar{w}) that we reanalyzed this time were the same as those in the previous studies. However, we now employ a different method in turbulence decomposition to analyze the characteristics of fluctuations, and hope to obtain some new results.

Figure 2 shows the 10-min averaged horizontal wind speed \bar{u} recorded by the cup anemometers at 6 levels and the ultrasonic anemometer at 1 level on the tower. Figure 2 captures the whole process of Hagupit, as observed by Zhizi station from 0000 BT 22 to 2400 BT 27 September, including the region of the typhoon

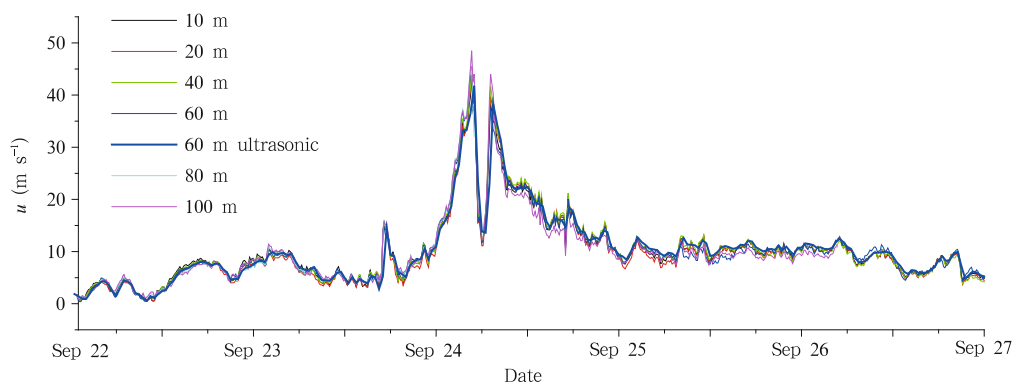


Fig. 2. Time series of 10-min averaged horizontal velocity \bar{u} at 6 levels by cup anemometers and 1 level by ultrasonic anemometer on the Zhizi tower during 22–24 September 2008.

eye, two regions of eye wall squall, and the outside field of the typhoon before (24 September) and after (25 September) its landing. Figure 3 shows \bar{u} and \bar{w} observed by the ultrasonic anemometer, but only for 24 September 2008.

These two figures indicate that the results of the cup anemometers and the ultrasonic anemometer are consistent. There are some clear characteristics in the average flow (\bar{u} , \bar{w}). Firstly, in the 20–110-m layer (above sea surface), \bar{u} is almost independent of height (note that by adding the data of the highest velocity from Bohe station during the typhoon's landing, we could conclude that \bar{u} from sea level to 110 m is the same). Only for a very short time during the period of strongest wind ($> 35 \text{ m s}^{-1}$) is there an exception—the difference between \bar{u} at the highest two levels is about 10 m s^{-1} . Secondly, at the 60-m level (70 m above the sea surface), there is upward motion ($\bar{w} > 0$); specifically, \bar{w} reaches 2–4 m s^{-1} at the squall wall, and 0.5–1 m s^{-1} in the typhoon eye region. The variable \bar{w} increases with \bar{u} . Only for a very short time after the typhoon's passage is \bar{w} reduced to nearly 0 m s^{-1} . This is an important point, and why \bar{w} is $> 0 \text{ m s}^{-1}$ is to be discussed in the last section of this paper. It should be noted that the observed \bar{w} is correct, because before and after the typhoon's passage the difference in wind direction is about 180° , but the observed \bar{w} does not change sign, and it is unlikely that the inclinometer has produced any error.

Figure 4 shows the pairs (\bar{u} , \bar{w}) and their regression. It can be seen that the accuracy of the regres-

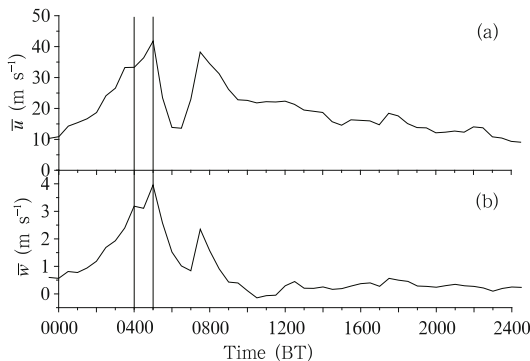


Fig. 3. (a) \bar{u} and (b) \bar{w} obtained by the ultrasonic anemometer at 60-m level of the Zhizi tower on 24 September 2008.

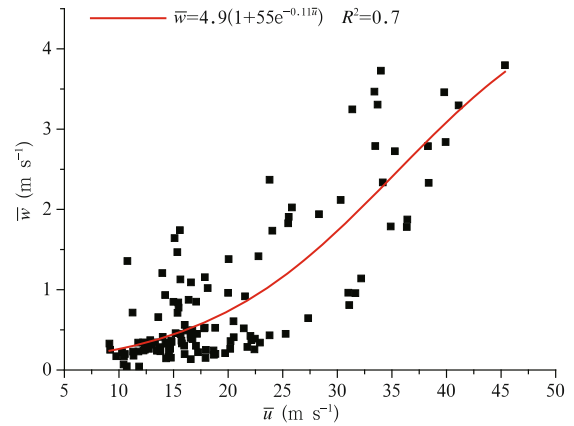


Fig. 4. Pair points (\bar{u} , \bar{w}) and their regression.

sion is high. Note that here \bar{u} is considered as the wind velocity at 10 m above sea surface, as suggested in the literature.

4. Characteristics of the turbulent fluctuations and gusty wind disturbances

The methods by Zeng et al. (2010) and Cheng et al. (2011, 2012a, 2014) are employed here to analyze the characteristics of fluctuations (u' , v' , w') of the ultrasonic anemometer data, where $u' = u - \bar{u}$; $v' = v$, $\bar{v} = 0$; $w' = w - \bar{w}$, and u is along the downwind direction. The averaging interval is 10 min. We further divide the fluctuations into two types: turbulent fluctuations (u_t , v_t , w_t) and gusty disturbances (u_g , v_g , w_g). The former consists of components with frequency $> 1/60 \text{ Hz}$, and the latter with frequency between $1/600$ and $1/60 \text{ Hz}$. The variable u_i ($i = t, g$) is along the 10-min averaged wind direction. The data are analyzed for the whole period, i.e., 22–27 September 2008, but with special attention paid to the strong wind period ($\bar{u} \geq 10 \text{ m s}^{-1}$).

Figure 5 shows the gusty disturbances u_g and turbulent fluctuations u_t for the eye wall squall period (0400–0500 BT 24 September 2008), as denoted by the two vertical lines in Fig. 3. It can be seen that the gusty disturbances and turbulent fluctuations are all quite strong. By using \bar{u} as the abscissa, the turbulence kinetic energy (E_t) and the gusty amplitude of the horizontal component (A_{gh}) are given in Figs. 6 and 7, respectively. Three direction components of

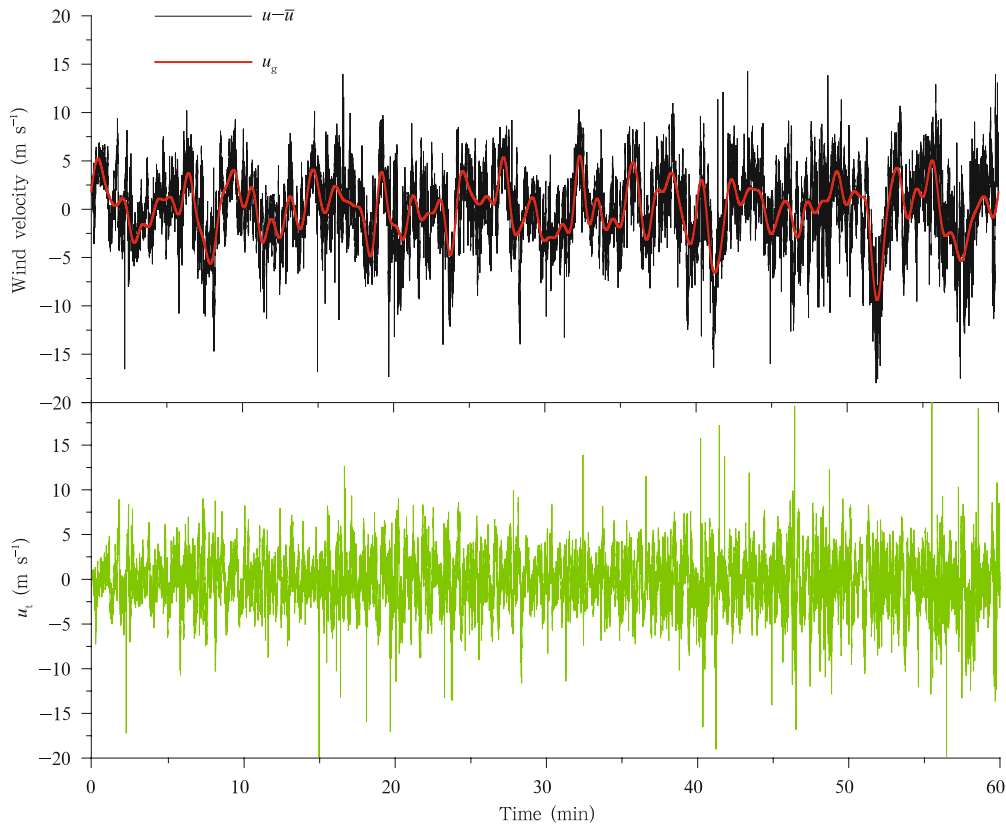


Fig. 5. Gusty disturbances u_g and turbulent fluctuations u_t during 0400–0500 BT 24 September 2008.

turbulence energy (E_{tu} , E_{tv} , E_{tw}) and three components of gusty amplitude (A_{gu} , A_{gv} , A_{gw}) are also given in Figs. 6 and 7, where $E_t = E_{tu} + E_{tv} + E_{tw}$, $A_{gh} = (A_{gu}^2 + A_{gv}^2)^{\frac{1}{2}}$, and the kinetic energy of gusts $E_{gi} = A_{gi}^2$, ($i = u, v, w$). It can be seen that during the strong wind period, the anisotropy of gusty disturbances ($A_{gu} > A_{gv} > A_{gw}$) is significant, and the turbulent fluctuations are also anisotropic to some extent, but weaker than that of gusts. This is a common characteristic of windy atmospheric layers, no matter if they are above the land surface (Zeng et al., 2010; Cheng et al., 2011) or above the oceanic surface (Cheng et al., 2014); however, during strong typhoons, this feature is the strongest.

The equivalent period of gusts (T_g , another useful index in practical applications) and its regression are given in Fig. 8. The frequency of the gusty wind disturbance is between 1/600 and 1/60 Hz. There are different periods of gusts in the atmospheric bound-

ary layer. The equivalent period of gusts refers to the main period of gusts by analyzing their power spectra. Note that the points in the region with $\bar{u} < 10 \text{ m s}^{-1}$ are scattered due to the randomness and spontaneity of gust occurrences during weak wind cases, but this does not lead to a serious problem in the practical application of the regression because gusts are weak and present only a small influence on heat and mass transport in such situations.

5. Friction velocity and vertical transport of momentum

Figure 9 is the superposition of u_g and w_g during 0400–0500 BT 24 September 2008. It shows very strong coherence at most moments: $u_g > 0$ is accompanied by $w_g < 0$, and $u_g < 0$ by $w_g > 0$. Therefore, the downward vertical flux of momentum, contributed by gusty disturbances, is large. The vertical flux of

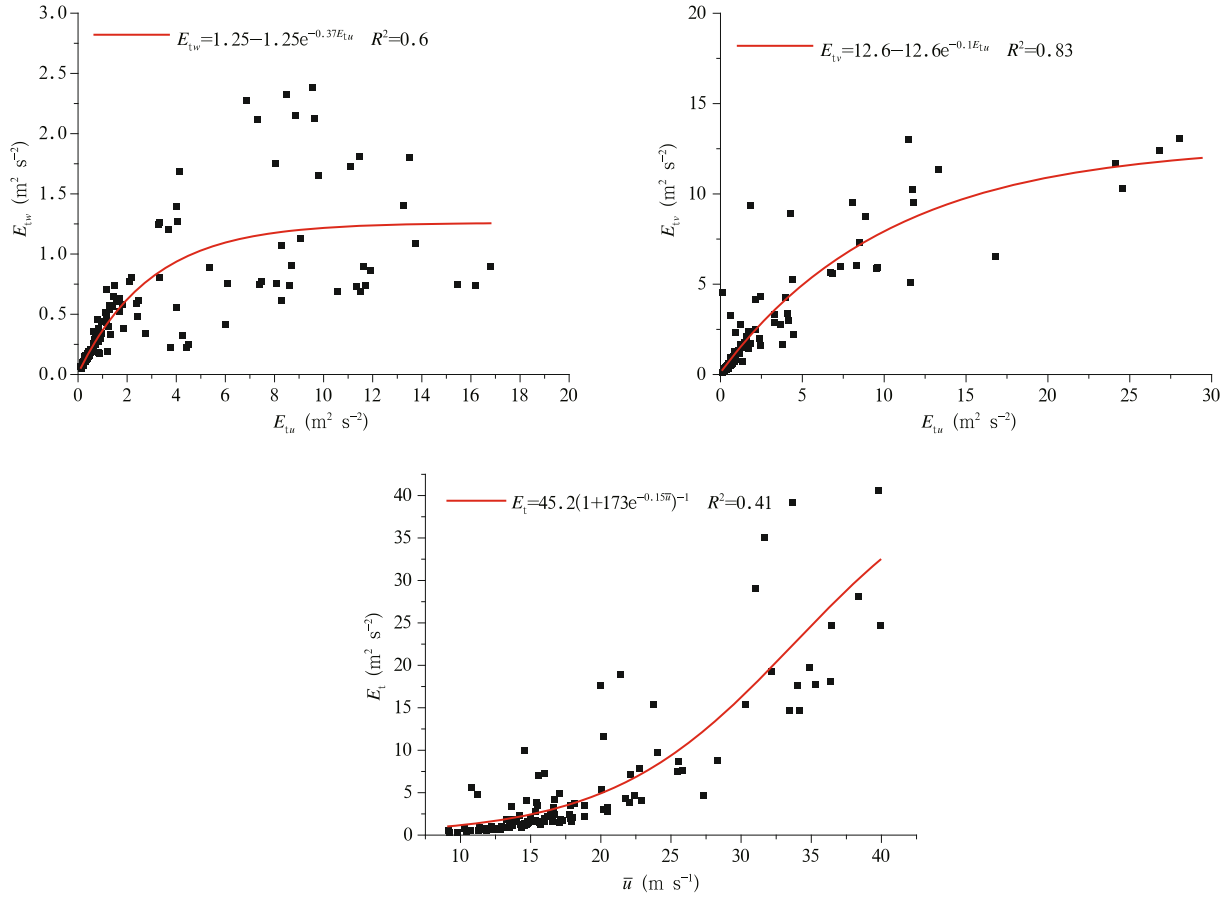


Fig. 6. Kinetic energy of turbulent fluctuation (E_t) and its three components (E_{tu} , E_{tv} , E_{tw}). The regressions are also given in solid lines.

momentum contributed by turbulent fluctuations is also downward. The absolute values of both parts of the momentum fluxes are equal to u_{g*}^2 and u_{t*}^2 , respectively. Figures 10a and 10b show respectively the gusty friction velocity (u_{g*}) and turbulent friction velocity (u_{t*}). Figures 10c and 10d also show u_* (the friction velocity in the conventional sense) and u_{m*} , where $u_*^4 \approx u_{g*}^4 + u_{t*}^4$ (Cheng et al., 2007), u_{m*} is called the average flow friction velocity, and the related momentum flux is $\bar{u} \cdot \bar{w}$, i.e., $u_{m*} = |\bar{u} \cdot \bar{w}|^{\frac{1}{2}}$. In the case of Hagupit, fluctuations cause downward fluxes of momentum, but the average flow causes upward flux. The upward momentum flux by the average flow is at least one order of magnitude larger than the downward momentum flux by fluctuations, although the latter is very much larger than that under weak wind conditions. It seems that the 10-min average motion is related to the transport of momentum from

ocean to the atmosphere during the typhoon period. Note that in strong wind situations, u_{g*} , u_{t*} , u_* , and even u_{m*} can be parameterized by \bar{u} , as shown by the high accuracy of the regressions in Fig. 10.

The sensible heat flux and latent heat flux are not given in this paper because the heat and water vapor exchanges between the atmosphere and the sea spray and spume generated by breaking waves and entrained into the atmospheric boundary layer are special subjects of research, and will thus be discussed in future work.

6. Summary and discussion

Analyses of the marine-atmospheric boundary layer during strong Typhoon Hagupit in September 2008 and the windy atmospheric boundary layer related to a cold surge in March 2012 over the South

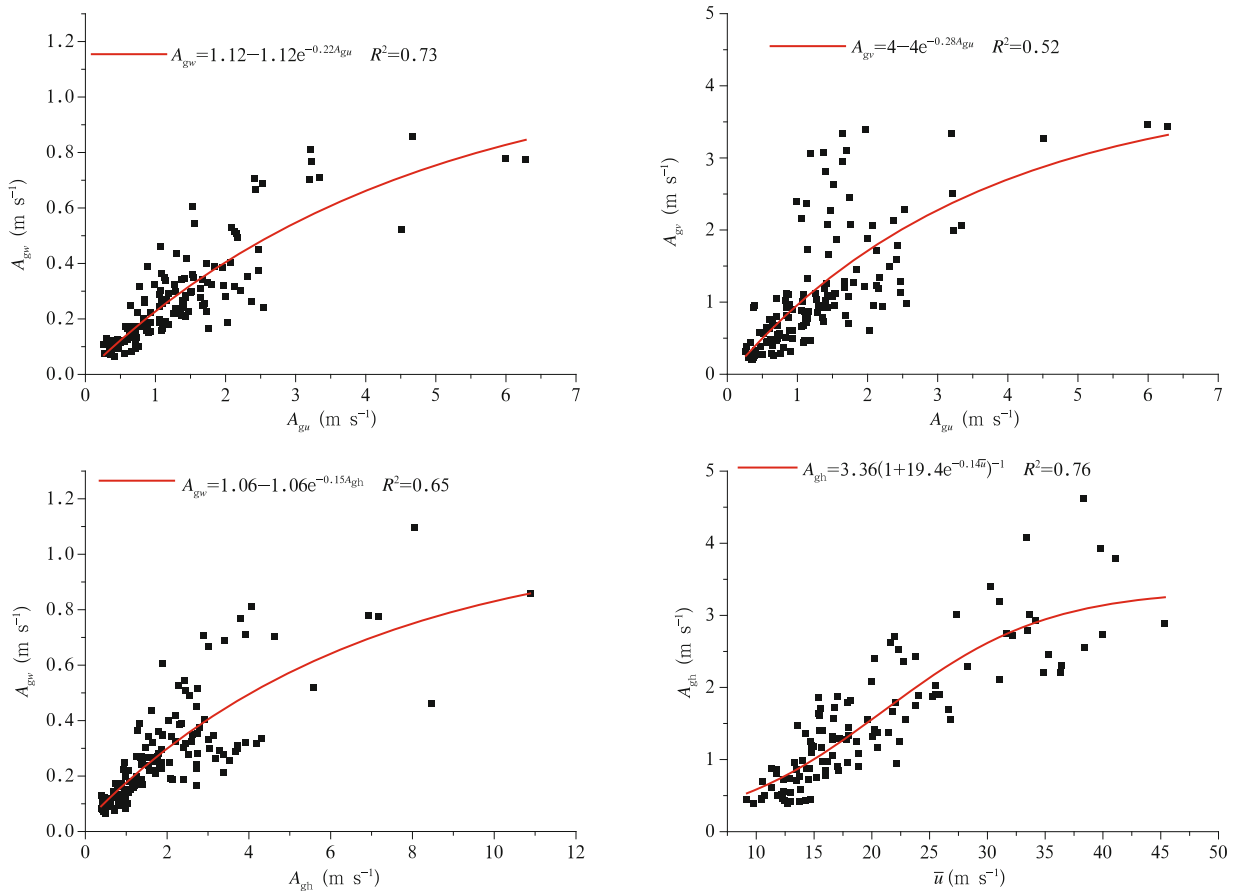


Fig. 7. Horizontal amplitude (A_{gh}) and its three component amplitudes (A_{gu} , A_{gv} , A_{gw}) of the gusty disturbances and associated regressions.

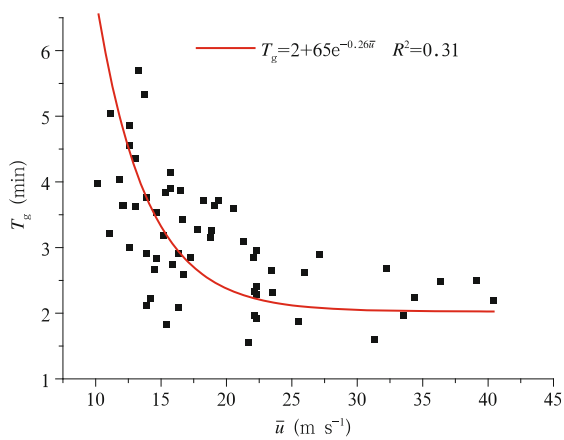


Fig. 8. The equivalent period of gusty disturbances (T_g) and the associated regression.

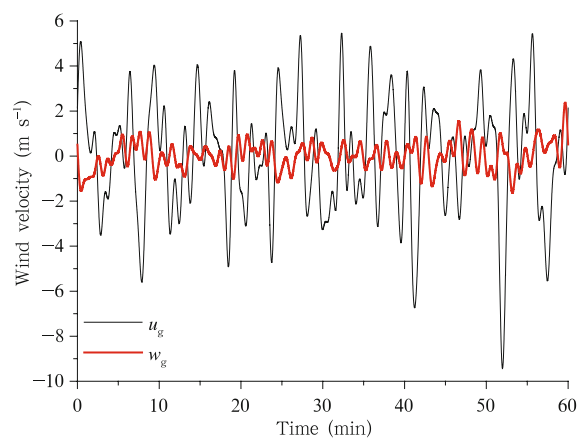


Fig. 9. Superposition of u_g (black line) and w_g (red line) during 0400–0500 BT 24 September 2008.

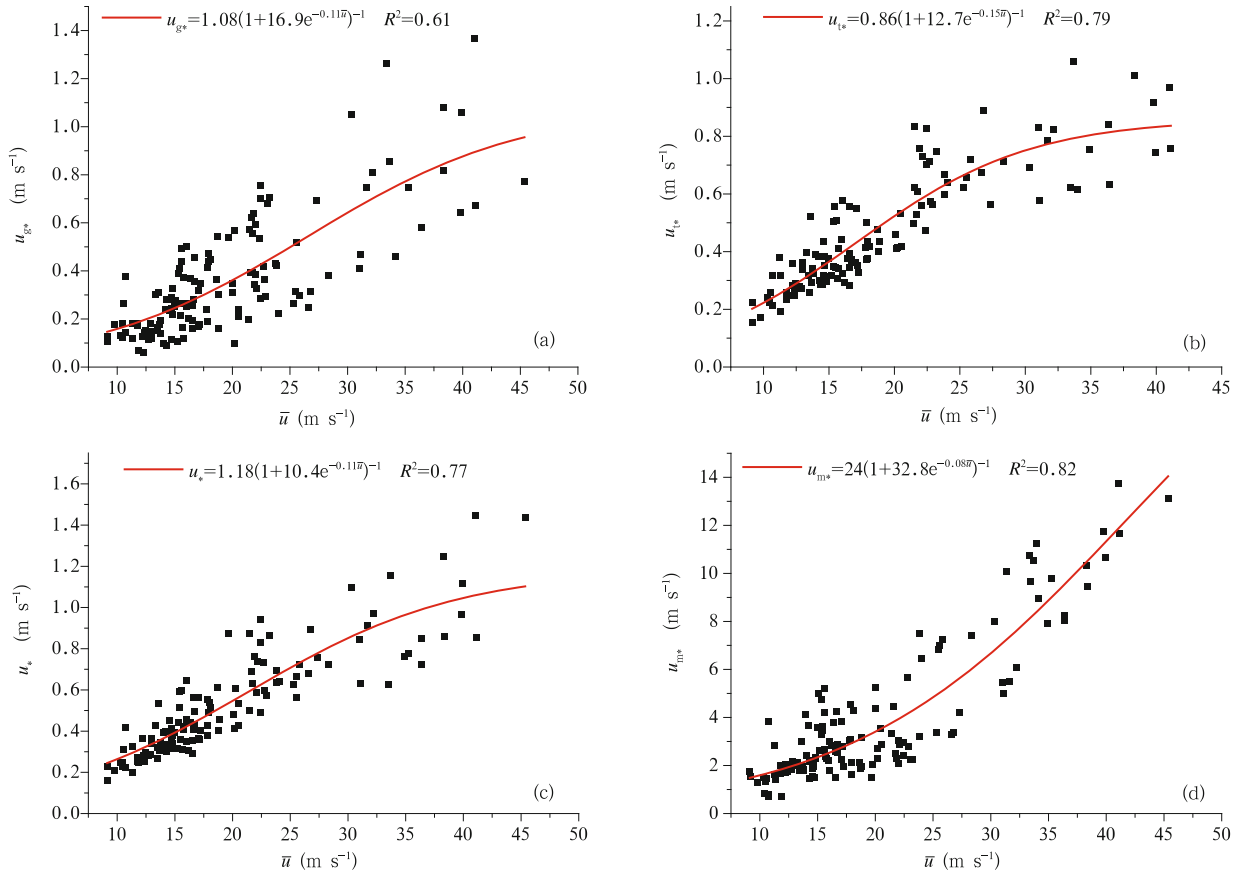


Fig. 10. Parameterized friction velocity. (a) Gusty friction velocity, (b) turbulent friction velocity, (c) friction velocity in the conventional sense, and (d) average flow friction velocity.

China Sea (Cheng et al., 2014) indicate that in the marine-atmospheric boundary layer during strong winds, the characteristics of both the average flow (\bar{u} , \bar{w}) and fluctuations (turbulences and gusts) possess many similarities but also some differences with those during the strong wind cases over the land surface (Zeng et al., 2010; Cheng et al., 2011). The major findings of the study can be summarized as follows.

(1) In the low-latitude marine-atmospheric boundary layer, during strong wind periods associated with tropical storms, hurricanes, or cold surges, the horizontal average velocity \bar{u} is almost independent of height below about 100 m, and the vertical velocity \bar{w} is greater than 0 m s^{-1} . This is different from land surface cases related to cold air mass outbreaks, where \bar{u} increases rapidly with height, and \bar{w} may be negative (descending cold air).

(2) During the strong wind periods, in the lower

part of the atmospheric layer, whether over the ocean or land, gusty wind disturbances are anisotropic and coherent, and turbulent fluctuations are also anisotropic to some extent (with vertical kinetic energy significantly less than the horizontal one) but with weak coherency.

(3) During strong wind periods, the energies of gusts (E_{gi}) and turbulences (E_{ti}) ($i = u, v, w$), as well as the corresponding friction velocities (u_{g*} and u_{t*}), are all much larger than those in weak-wind situations. The vertical fluxes of momentum contributed by gusts and turbulences are all downward. They can be parameterized by using \bar{u} as the controlling factor in marine boundary layer cases because of the independence of \bar{u} to height. However, the top height of our observations is not sufficient for obtaining their vertical profiles.

(4) According to our analysis of observational

data, strong wind is accompanied by upward vertical velocity in the marine-atmospheric boundary layer, and \bar{w} is $\geq 0.25 \text{ m s}^{-1}$ when \bar{u} is $\geq 10 \text{ m s}^{-1}$, and \bar{w} is $\geq 1.0 \text{ m s}^{-1}$ when $\bar{u} \geq 30 \text{ m s}^{-1}$. This means that the upward transport of horizontal momentum, $\bar{u} \cdot \bar{w}$, is ≥ 2.5 and $\geq 30.0 \text{ m}^2 \text{ s}^{-2}$, respectively. These values are at least one order of magnitude larger than the downward fluxes due to the fluctuations ($u_*^2 = 0.04$ and $0.6 \text{ m}^2 \text{ s}^{-2}$, respectively). This fact is important and should be further studied because strong wind occurs frequently above the marine surface. Generally speaking, we can imagine that strong wind (average atmospheric flow) and the superimposed fluctuations drive oceanic surface currents and generate large breaking waves. Thus, a marine-atmosphere coupled boundary layer is formed, and on the atmospheric side, the boundary layer is different from that over the land, and some portion of the sea momentum can be fed back to the atmosphere from the ocean. This may be the reason why \bar{u} is independent of height. Furthermore, the sea spray and spume droplets make special exchanges of heat and mass transport between the ocean and atmosphere.

From the reanalysis data of the ECMWF, NCEP, and GFDL (Geophysical Fluid Dynamics Laboratory), we can see that in the middle and high latitudes $\bar{w} \geq 0$ (i.e., $\omega \equiv dP/dt \leq 0$) at 10 m over a broad area of the oceanic surface when there is a mature cyclone passing over, and $\bar{w} \leq 0$ (i.e., $\omega > 0$) occurs only in the cold frontal region near the center of the cyclone. If this can be confirmed by observations, it might be true that $\bar{w} \geq 0$ at 10 m occurs very often and covers most of the oceanic surface areas during strong winds.

Another concern is about the 10-m wind. According to the Beaufort scale, when the 10-m wind is force 8 (17.2–20.7 m s^{-1}), force 10 (24.5–28.4 m s^{-1}), and force 12 (hurricane; 32.7–36.9 m s^{-1}), the significant wave heights are 5.5 (usual) to 7.5 m (highest), 9.0 (usual) to 12.5 m (highest), and 14.0 (usual) to > 16.0 m (highest), respectively. Therefore, the so-called 10-m wind above the oceanic surface is actually meaningless. Fortunately, \bar{u} is independent of height in the strong wind situation.

Acknowledgments. We are very grateful to

the Guangdong Meteorological Bureau for providing some data.

REFERENCES

- Aberson, S. D., M. L. Black, R. A. Black, et al., 2006: Thirty years of tropical cyclone research with the NOAA P-3 aircraft. *Bull. Amer. Meteor. Soc.*, **87**, 1039–1055.
- Cao, S. Y., Y. Tamura, N. Kikuchi, et al., 2009: Wind characteristics of a strong typhoon. *J. Wind Eng. Indust. Aerodyn.*, **97**, 11–21.
- Chen, W. C., L. L. Song, S. Q. Zhi, et al., 2011: Analysis on gust factor of tropical cyclone strong wind over different underlying surfaces. *Sci. China (Tech. Sci.)*, **54**, 2576–2586.
- Cheng, X. L., Q. C. Zeng, and F. Hu, 2011: Characteristics of gusty wind disturbances and turbulent fluctuations in windy atmospheric boundary layer behind cold fronts. *J. Geophys. Res. Atmos.*, **116**, D06101, doi: 10.1029/2010JD015081.
- , —, and F. Hu, 2012a: Parameterizations of some important characteristics of turbulences and gusts in the atmospheric boundary layer. *J. Geophys. Res. Atmos.*, **117**, D08113.
- , —, and —, 2012b: Stochastic modeling of the effect of wind gust on dust entrainment during sand storms. *Chinese Sci. Bull.*, **57**, 3595–3602.
- , J. Huang, L. Wu, et al., 2014: Structures and characteristics of windy atmospheric boundary layer in the South China Sea region during cold surge. *Adv. Atmos. Sci.* (in press)
- Cheng Xueling, Zeng Qingcun, Hu Fei, et al., 2007: Gustiness and coherent structure of strong winds in the atmospheric boundary layer. *Climatic Environ. Res.*, **12**, 227–243. (in Chinese)
- Franklin, J. L., M. L. Black, and K. Valde, 2002: GPS dropwindsonde wind profiles in hurricanes and their operational implications. *Wea. Forecasting*, **18**, 32–44.
- French, J. R., W. M. Drennan, J. A. Zhang, et al., 2007: Turbulent fluxes in the hurricane boundary layer. Part I: Momentum flux. *J. Atmos. Sci.*, **64**, 1089–1102.
- Haper, B. R., 2008: Wind speed time averaging conversions for tropical cyclone conditions. 28th Conference on Hurricanes and Tropical Meteorology, Amer. Meteor. Soc., Orlando, FL, No. 4B1.

- Knupp, K. R., J. Walters, and M. Biggerstaff, 2005: Doppler profiler and Radar observations of boundary layer variability during the landfall of tropical storm Gabrielle. *J. Atmos. Sci.*, **63**, 234–251.
- Kudryavtsev, V. N., and V. K. Makin, 2007: Aerodynamic roughness of the sea surface at high winds. *Boundary-Layer Meteor.*, **125**, 289–303.
- Li Qiusheng, Dai Yimin, Li Zhengnong, et al., 2010: Surface layer wind field characteristics during a severe typhoon ‘Hagupit’ land falling. *J. Building Structures*, **31**, 54–61. (in Chinese)
- Liu Donghai, Song Lili, Li Guoping, et al., 2011: Analysis of the extreme loads on offshore wind turbines by strong Typhoon Hagupit. *J. Trop. Meteor.*, **27**, 317–326. (in Chinese)
- Ola, P., G. Persson, J. E. Hare, et al., 2005: Air-sea interaction processes in warm and cold sectors of extratropical cyclonic storms observed during FASTEX. *Quart. J. Roy. Meteor. Soc.*, **131**, 877–912.
- Peng Zhen, Song Lili, Hu Fei, et al., 2012: Multi-scale analysis on momentum flux of Typhoon Chanchu during its landfall. *J. Trop. Meteor.*, **28**, 61–67. (in Chinese)
- Powell, M. D., P. J. Vickery, and T. A. Reinhold, 2003: Reduced drag coefficient for high wind speeds in tropical cyclones. *Nature*, **422**, 279–283.
- Sanford, T. B., J. F. Price, J. B. Girton, et al., 2007: Highly resolved observations and simulations of the ocean response to a hurricane. *Geophys. Res. Lett.*, **34**, L13604, doi: 10.1029/2007GL029679.
- Schroeder, J. L., and S. Douglas, 2003: A hurricane bonnie wind flow characteristics as determined from WEMITE. *J. Wind Eng. Indust. Aerodyn.*, **91**, 767–789.
- Song Lili, Mao Huiqin, Huang Haohui, et al., 2005: Analysis on boundary layer turbulent features of land-falling typhoon. *Acta Meteor. Sinica*, **63**, 915–921. (in Chinese)
- , Pang Jiabin, Jiang Chenglin, et al., 2010: Field measurement and analysis of turbulence coherence for Typhoon Nuri at Macao Friendship Bridge. *Sci. China (Tech. Sci.)*, **53**, 2647–2657.
- Sparks, P. R., 2001: Wind speeds in tropical cyclones and surface-to-gradient wind-speed ratios in tropical cyclones. *J. Wind Eng. Indust. Aerodyn.*, **89**(11–12), 1047–1058.
- Xiao Yiqing, Li Lixiao, Song Lili, et al., 2012: Study on wind characteristics of Typhoon Hagupit based on offshore sea surface measurements. *Acta Aerodyn. Sinica*, **30**, 380–387. (in Chinese)
- Xu, Y. L., and S. Zhan, 2001: Field measurements of Diwang Tower during Typhoon York. *J. Wind Eng. Indust. Aerodyn.*, **89**, 73–93.
- Zedler, S. E., P. P. Niiler, D. Stammer, et al., 2009: Ocean’s response to Hurricane Frances and its implications for drag coefficient parameterization at high wind speeds. *J. Geophys. Res. Oceans*, **114**, C04016, doi: 10.1029/2008JC005205.
- Zeng Qingcun, 2006: *Gigantic Yellow Cloud—The Dust Storm in Eastern Asia*. Science Press, Beijing, 228 pp. (in Chinese)
- , Cheng Xueling, Hu Fei, et al., 2010: Gustiness and coherent structure of strong winds and their role in the dust emission and entrainment. *Adv. Atmos. Sci.*, **27**, 1–13.
- Zhang, J. A., P. G. Black, J. R. French, et al., 2008: First direct measurements of enthalpy flux in the hurricane boundary layer: The CBLAST results. *Geophys. Res. Lett.*, **35**, L14813. doi: 10.1029/2008GL034374.